THE JOURNAL OF PHYSICAL CHEMISTRY B

Article

pubs.acs.org/JPCB

Comparative Study of Imidazolium- and Pyrrolidinium-Based Ionic Liquids: Thermodynamic Properties

Yoshitaka Shimizu,*[,†,‡] Yoko Ohte,[†] Yasuhisa Yamamura,[‡] Seiji Tsuzuki,[§] and Kazuya Saito[‡]

[†]National Metrology Institute of Japan, National Institute of Advanced Industrial Science and Technology, Tsukuba Central 3, 1-1-1 Umezono, Tsukuba, Ibaraki 305-8563, Japan

[‡]Department of Chemistry, Faculty of Pure and Applied Sciences, University of Tsukuba, Tsukuba, Ibaraki 305-8571, Japan

[§]Nanosystem Research Institute, National Institute of Advanced Industrial Science and Technology, Tsukuba Central 2, 1-1-1 Umezono, Tsukuba, Ibaraki 305-8568, Japan

Supporting Information

ABSTRACT: Heat capacities of liquid, crystal(s) and liquid-quenched glass (LQG) of room-temperature ionic liquid 1-butyl-3-methylimidazolium bis(trifluoromethylsulfonyl)amide ([bmim][Tf_2N]) and *N*-butyl-*N*-methylpyrrolidinium bis(trifluoromethylsulfonyl)amide ([bmp][Tf_2N]) were measured by adiabatic calorimetry. The melting points of [bmim][Tf_2N] and [bmp][Tf_2N] were 270.42 and 265.82 K, respectively. Heat capacity anomalies depending on thermal history after crystallization were observed above 200 K in both compounds. Two thermal anomalies due to glass transitions in crystalline [bmim][Tf_2N] were observed at 59 and 73 K. One thermal anomaly independent of thermal history was observed in a metastable crystalline [bmp][Tf_2N]. Thermal properties related to LQG of [bmim][Tf_2N] and [bmp][Tf_2N] are similar to those of other glass formers, and they are classified as fragile liquids. Heat capacities of $[bmim]^+$ and $[bmp]^+$ due to normal modes of the intramolecular vibration were evaluated through DFT calculations. The comparison between experimental and calculated heat capacity differences shows that the trends in the liquid phase are consistent with each other, while those in the crystal phase deviate further as the temperature is increased. This result supports the authors' previous conclusion that the origin of the low melting point is not a curious property of the liquid but primarily related to properties of the crystal.

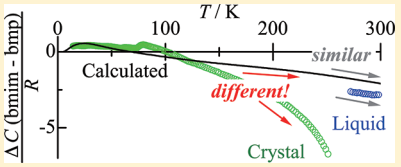

1. INTRODUCTION

Ionic liquids attract many researchers. Indeed, in progress are many researches aiming at practical applications utilizing their characteristics.[1,2] To have more useful ionic liquids, new ionic liquids are pursued by the variation in combination of existing cations and anions or by the synthesis of new cations and/or anions. However, substitution of ions with useful physical properties often brings about results against the expectation, such as a significant increase of melting points.[3] Balances among physical and electrical properties are also important for practical ionic liquids.

Predicting physical properties is one of the most important issues for the design of new ionic liquids.[4−7] Group contribution method (GCM)[8−10] and the quantitative structure−property relationship (QSPR)[11−19] are typical techniques for the prediction. Also used are molecular simulations, which in principle should be capable of reproducing any properties on the basis of microscopic interaction/dynamics.[20−22] In GCM, physical properties are predicted by applying a model deduced from the correlation of physical properties with the molecular (ionic) structure, whereas models with descriptors reflecting the molecular properties such as structure, polarity, and energy state are used in QSPR. Goodness of the resulting predictions is primarily determined by the input data used for establishing the model. For ionic liquids, large scatter among reported data of the same physical property by different researchers has often been pointed out.[23] This is why the IUPAC conducted the project on measurement of thermodynamic and transport properties of 1-hexyl-3-methylimidazolium bis(trifluoromethylsulfonyl)amide ([hmim][Tf_2N]) as the reference sample for standardization of physical property measurements.[24,25] We took part in the IUPAC project and measured the heat capacity. This paper is a contribution utilizing adiabatic calorimetry, which has long been regarded as the most accurate in determining thermodynamic quantities.

The same series of ionic liquids as [hmim][Tf_2N], 1-alkyl-3-methylimidazolium bis(trifluoromethylsulfonyl)amide ([$C_n$mim][Tf_2N]; n is the number of carbon atoms in an alkyl chain) is one of the best-known ionic liquids because of its stability in the atmosphere at room temperature.[2,26] We have studied thermodynamic properties of some of [$C_n$mim][Tf_2N] by using adiabatic calorimetry.[27−29] From the alkyl chain length dependence of the thermodynamic properties, the origin of the low melting point of [$C_n$mim][Tf_2N] with a short alkyl chain was identified as the low entropy of the crystal.[29] This result demonstrates the importance of study on not only liquid but also solid states.

Received: November 5, 2011
Revised: April 5, 2012
Published: April 27, 2012

   dx.doi.org/10.1021/jp210626v | *J. Phys. Chem. B* 2012, 116, 5406−5413

To demonstrate the wide applicability of reasoning why the unique properties relevant to low melting point reside in the crystal rather than the liquid, we decided to extend the object of our study to other series of ionic liquids. Focusing on the aromatic property of the imidazolium cation, we chose a pyrrolidinium cation as a nonaromatic cation while the anion was fixed at $[Tf_2N]^-$. Both cations are quaternary ammonium of low symmetry consisting of a five-membered ring and the same alkyl chains. The butyl chain was chosen because various cations with butyl chain have widely been studied. According to existing literature,[30−34] [bmim][Tf_2N] and [bmp][Tf_2N] exhibit similar thermodynamic and physical properties such as glass transition temperature, melting point, thermal expansion coefficient of the liquid, and the density of the liquid. In this paper, the results of precise calorimetry are compared between them in detail. Although some of the corresponding data have already been reported on the basis of adiabatic calorimetry,[35,36] the present data still deserve publication to establish the reliable database. It is also noted that the detailed analysis described below needs precise data obtained from the same calorimeter.

In a previous paper,[37] one of the present authors showed, on the basis of ab initio calculations, that the interaction between a cation and an anion of 1-ethyl-3-methylimidazolium tetrafluoroborate ([emim]·BF_4) is not very different from that of *N*-ethyl-*N*-methylpyrrolidinium tetrafluoroborate ([emp]·BF_4), in contrast to a large difference in melting point (14[38] and 280 °C[39]). A similar interaction is expected for the ion pair in the present case, accordingly. [bmim][Tf_2N] and [bmp][Tf_2N] have the same alkyl chains in their cations. Due to the difference in the cation, the following factors may affect the *bulk* properties: existence of charge delocalization, steric effects owing to alkyl chains, and bond orders. Delocalization of charge in (aromatic) cation and steric effects of the alkyl chain would cause a small change in the cation−anion interaction and influence thermodynamic properties, especially concerning fusion. The difference in the bond orders between the imidazolium ring and pyrrolidinium ring brings about the difference in thermodynamic quantities owing to contributions of intramolecular vibrations. To clarify the contribution of intramolecular vibrations, vibrational analyses of $[bmim]^+$ and $[bmp]^+$ were performed. Effects of the intermolecular interaction on the thermodynamic properties of [bmim][Tf_2N] and [bmp][Tf_2N] are discussed through the comparisons between experimental and calculated heat capacities.

2. EXPERIMENTAL SECTION

[bmim][Tf_2N] (molar mass: 419.36 g mol^{-1}) was purchased from Solvent Innovation (Lot. 99/748). The sample was washed with *n*-hexane and pure water and then dried in a vacuum oven at 50 °C for more than 12 h. The water content was measured by coulometric Karl Fischer titration (AQ-7, Hiranuma Sangyo Co., Ltd.) to be 110 mg/kg. The dried [bmim][Tf_2N] (6.7166 g) was loaded into a chromium-plated copper calorimeter vessel (vessel 1) under a helium atmosphere.

[bmp][Tf_2N] (molar mass: 422.41 g mol^{-1}) was purchased from Kanto Chemicals (Lot. No. 811062). The sample was dried in a vacuum oven at 50 °C for 16 h. The water content by coulometric Karl Fischer titration (AQ-2100, Hiranuma Sangyo Co., Ltd.) was 100 mg/kg. The dried [bmp][Tf_2N] (5.6558 g) was loaded into a chromium-plated copper calorimeter vessel (vessel 2) under a helium atmosphere.

Heat capacities of [bmim][Tf_2N] and [bmp][Tf_2N] were measured by an adiabatic calorimeter (JECC Torisha Co., Inc. JTA-2000C) in the heating direction. While the working thermometer mounted to vessel 1 was a commercial platinum resistance thermometer (Tinsley 5187 L) calibrated at the National Physical Laboratory (NPL) of U.K., that of vessel 2 was a commercial rhodium−iron resistance thermometer (Tinsley 5187U) calibrated at NPL (0.65−27.1 K) and Oxford Instruments (27−300 K). Their temperature scales were based upon the ITS-90.[40] The same calorimeter was used for the measurement on [hmim][Tf_2N] in the IUPAC project, the result of which was reported with detailed analysis of experimental uncertainties.[27]

Contributions of [bmim][Tf_2N] ([bmp][Tf_2N]) to the total heat capacity including that of the calorimeter vessel were 69 (70), 40 (36), 32 (31), 35 (35), and 44% (43%) at 15, 50, 100, 200, and 300 K, respectively. Times needed for thermal equilibrium of the [bmim][Tf_2N] ([bmp][Tf_2N]) were 5 (5), 20 (15), 20 (20), 10 (10), and 10 min (10 min) at 15, 50, 100, 200, and 300 K, respectively. Relative uncertainties, which correspond to the half-width of an estimated confidence interval of approximately 95% of the calorimetric results above 80 K, did not exceed 0.8%.

Vibrational analyses for isolated $[bmim]^+$ and $[bmp]^+$ were carried out by density functional theory (DFT) calculations at the B3LYP/6-311+G** level using the Gaussian 03 program.[41] DFT calculations were performed for the most stable conformations of the two cations (*gauche−trans* $[bmim]^+$ and *trans−trans* $[bmp]^+$)[42] and for the *trans−trans* $[bmim]^+$. Molecular structures of the conformers are shown in Figure 1.

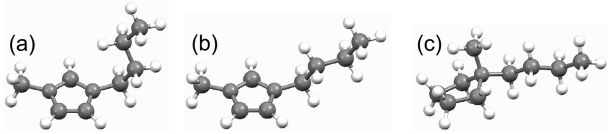

Figure 1. Molecular structures of conformers of $[bmim]^+$ and $[bmp]^+$ for DFT calculations: (a) *gauche−trans* $[bmim]^+$; (b) *trans−trans* $[bmim]^+$; (c) *trans−trans* $[bmp]^+$.

3. RESULTS

Purity Assay by the Freezing Point Depression Method. Purities of [bmim][Tf_2N] and [bmp][Tf_2N] were determined by the fractional melting method based on the melting point[43] depression caused by (unidentified) impurities in the sample.[27,44,45] Becuase the van't Hoff plots (Figures S1 and S2 in the Supporting Information) indicated the formation of a solid solution, melting point depression and the melting point of a pure sample of both ionic liquids were determined after the correction, assuming formation of a solid solution.[45] The purity in the amount of substance fraction (mole fraction), melting points of the pure substance and the calorimetric sample of [bmim][Tf_2N] ([bmp][Tf_2N]) were 0.997 mol mol^{-1} (0.997 mol mol^{-1}), 270.42 K (265.82 K), and 270.34 K (265.73 K), respectively.

Thermodynamic Properties of [bmim][Tf_2N]. Heat capacities (C_p) of a liquid, stable crystal and liquid-quenched glass (LQG) of [bmim][Tf_2N] are shown in Figure 2. Evaluated thermodynamic properties concerning the phase behavior are tabulated in Table 1 together with literature values

dx.doi.org/10.1021/jp210626v | J. Phys. Chem. B 2012, 116, 5406−5413

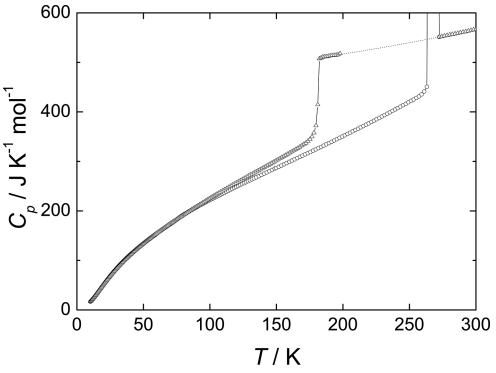

Figure 2. Heat capacities of liquid, crystal, and LQG of [bmim][Tf_2N]: circle, crystal; triangle, LQG and liquid.

Table 1. Thermodynamic Properties of [bmim][Tf_2N] and [bmp][Tf_2N][a]

thermodynamic properties	[bmim][Tf_2N][32]	[bmp][Tf_2N][33]
	Liquid	
$C_{p,liq}$(298.15 K)/J K^{-1} mol^{-1}	565.6 (566.2)	589.5 (588.0[b])
	Fusion	
T_{fus}/K	270.35 (270.22)	265.73 (265.65)
$\Delta_{fus}H$/kJ mol^{-1}	23.8 (23.78)	21.9 (21.9)
$\Delta_{fus}S$/J K^{-1} mol^{-1}	88.0 (88.0[b])	82.4 (82.4[b])
	Solid−Solid Phase Transition	
T_{tr}/K		140
$\Delta_{tr}H$/J mol^{-1}		200
$\Delta_{tr}S$/J K^{-1} mol^{-1}		1.5
	Glass Transition (LQG)	
T_g/K	180 (181.5)	181
$\Delta_{gl}C_p(T_g)$/J K^{-1} mol^{-1}	158 (155)	134
$\Delta_{gl}C_p(T_g)/C_p$(glass, T_g)	0.45 (0.43[b])	0.35
T_k/K		149
D		8.4
$S_c(T_g)$/J K^{-1} mol^{-1}		35
Z		4
S_{res}/J K^{-1} mol^{-1}		13

[a]Quantities in parentheses are the literature values. [b]Quantities are evaluated from the equation or related quantities in the literature.

from adiabatic calorimetry.[35] Resultant standard thermodynamic quantities at round temperatures are tabulated in Table 2. There are no thermal anomalies in the liquid phase. The heat capacity of the liquid at 298.15 K ($C_{p,liq}$(298.15 K)) is 565.6 J K^{-1} mol^{-1}, obtained from a quadratic polynomial fit to experimental heat capacities of the liquid.

Cooling at the cooling rate of ~1 K min^{-1} of the liquid (quenched sample) brought [bmim][Tf_2N] into LQG. The heat capacity jump owing to the glass transition was observed at around 180 K. The heat capacity jump, $\Delta_{gl}C_p(T_g)$ and its ratio against the C_p of LQG at the glass transition temperature (T_g), $\Delta_{gl}C_p(T_g)/C_p$(LQG,T_g), of the quenched sample are 158 J K^{-1} mol^{-1} and 0.45, respectively. The ratio is comparable with that of [hmim][Tf_2N].[27] [bmim][Tf_2N] is thus classified into the so-called "fragile liquid".[27,46]

The temperature drifts around the glass transition of LQG with the same equilibration periods are shown in Figure 3. The glass transition temperature is determined to be 180 K from the temperature where the temperature drift of the quenched sample becomes zero changing from exothermic to endothermic. After annealing at 178 K (where the largest exothermic

Table 2. Standard Thermodynamic Quantities of Glassy Crystal and Liquid of [bmim][Tf_2N]

T/K	C_p/ J K^{-1} mol^{-1}	$[H(T) - H(0)]T^{-1}$/ J K^{-1} mol^{-1}	$[S(T) - S(0)^a]$/ J K^{-1} mol^{-1}	$-[G(T) - H(0)]T^{-1}$/ J K^{-1} mol^{-1}
		Crystal		
15	32.63	11.39	16.59	5.20
20	51.02	19.00	28.50	9.50
25	68.43	27.16	41.77	14.61
30	84.33	35.39	55.68	20.29
35	98.50	43.41	69.77	26.36
40	111.17	51.10	83.76	32.66
45	122.69	58.43	97.53	39.10
50	133.22	65.39	111.01	45.62
55	143.78	72.09	124.26	52.17
60	153.68	78.48	137.20	58.72
65	163.56	84.64	149.89	65.25
70	172.20	90.60	162.34	71.74
75	182.48	96.39	174.58	78.19
80	192.37	102.09	186.68	84.59
90	207.6	113.0	210.2	97.2
100	221.9	123.2	232.8	109.6
110	235.5	132.8	254.6	121.8
120	248.7	141.9	275.7	133.8
130	261.7	150.6	296.1	145.5
140	274.4	159.0	316.0	157.0
150	286.9	167.1	335.3	168.2
160	299.5	175.0	354.2	179.2
170	312.2	182.7	372.8	190.1
180	324.9	190.2	391.0	200.8
190	337.7	197.6	408.9	211.3
200	350.7	205.0	426.5	221.5
210	364.0	212.2	444.0	231.8
220	377.8	219.4	461.2	241.8
230	391.5	226.6	478.3	251.7
240	405.7	233.8	495.3	261.5
250	420.2	240.9	512.1	271.2
260	435.0	248.1	528.9	280.8
270	450.0	255.3	545.6	290.3
270.35	450.5	255.6	546.2	290.6
		Liquid		
270.35	550.3	343.6	634.2	290.6
280	555.5	350.8	653.6	302.8
290	561.0	358.0	673.2	315.2
300	566.7	364.8	692.3	327.5

[a]$S(0)$ is not 0, owing to the frozen-in disorders in glassy crystal.

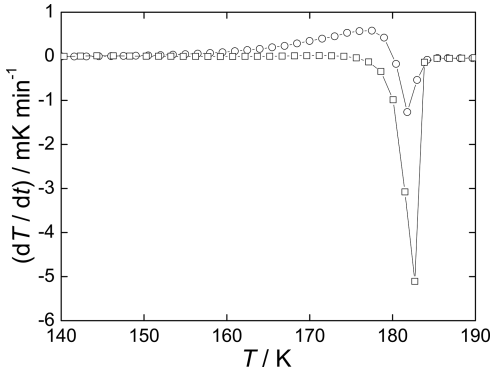

Figure 3. Temperature drifts of quenched and annealed LQG of [bmim][Tf_2N]: circle, quenched sample; square, annealed sample.

dx.doi.org/10.1021/jp210626v | J. Phys. Chem. B 2012, 116, 5406−5413

effect was observed) until the exothermic effect ceased, the heat capacity was measured again (annealed sample). The temperature drifts during the equilibration period of the quenched and annealed samples show characteristic temperature dependence due to the so-called enthalpy relaxation around the glass transition temperature.[27] The heat capacity of the annealed sample was slightly smaller than that of the quenched sample around the glass transition temperature.

Above the glass transition temperature, the supercooled liquid began to crystallize with an exothermic effect. After the crystallization with sufficient annealing (for more than 12 h in typical experiments), only one stable crystal phase was realized. A thermal anomaly with variation of the heat capacity and the spontaneous endothermic effect was detected for the crystal above 200 K. This thermal anomaly depended on their thermal history after crystallization, as reported previously.[28] The heat capacity shown in Figure 2 was obtained for the sample after heating to the middle of fusion.

In addition to this thermal anomaly, two thermal anomalies were observed below 80 K for the crystal. Both thermal anomalies are due to glass transitions with slight heat capacity jumps. The C_p/T around two glass transitions is shown in Figure 4. Temperature drifts in the same temperature range are

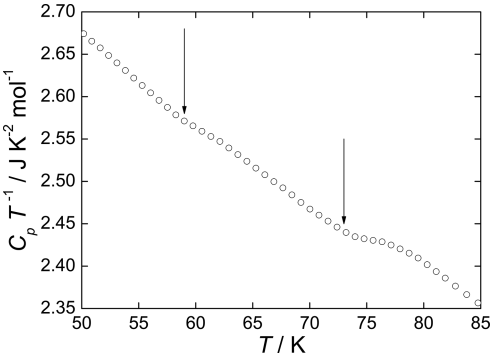

Figure 4. C_pT^{-1} around glass transitions in the crystal of [bmim][Tf_2N]: arrow, glass transition temperature.

shown in Figure 5. Their glass transition temperatures are 59 and 73 K, determined in the same manner as that for LQG. Both glass transitions observed in the crystal showed the so-called enthalpy relaxation as in LQG. Observation of the glass

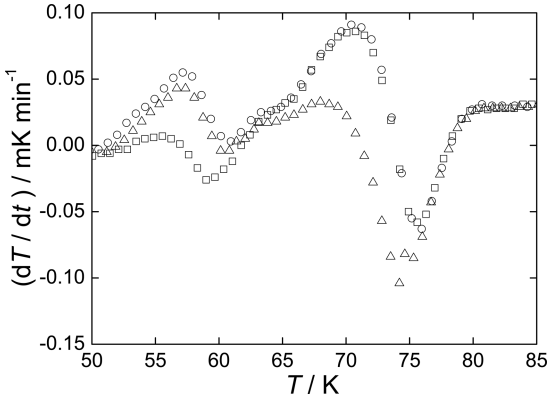

Figure 5. Temperature drifts around glass transitions in the crystal of [bmim][Tf_2N]: circle, quenched sample; square, annealed at 57 K; triangle, annealed at 70 K.

transition implies that the crystalline phase below these temperatures is the so-called "glassy crystal".[47] Although the origin of the disorder in this glassy crystal cannot be identified by calorimetry, the presence of disorder is in accordance with the assumption of disorder in the conformation of a butyl chain from the IR spectrum by Paulechka et al.[48] Because some disorder is certainly frozen in at low temperatures, analyses through the absolute entropy are not applicable to this compound, in contrast to [hmim][Tf_2N][27] and [bmp][Tf_2N] given below.

Fusion of this crystal was observed at 270.35 K. The enthalpy and entropy of fusion were 23.8 kJ mol^{-1} and 88.0 J K^{-1} mol^{-1}, respectively. The ratio of the glass transition temperature of LQG to the melting point was ~2/3. This ratio is almost the same as other glass-forming molecular liquids.[49]

Thermodynamic Properties of [bmp][Tf_2N]. Heat capacities of a liquid, stable crystal, metastable crystal, and LQG of [bmp][Tf_2N] are shown in Figure 6. Evaluated

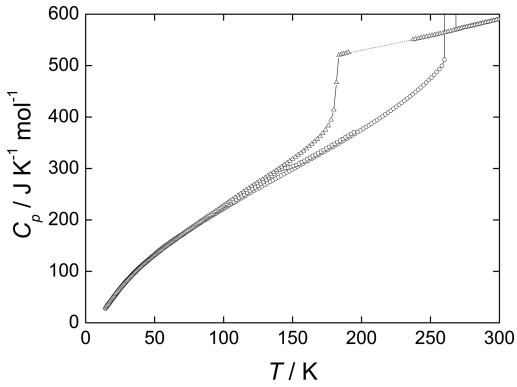

Figure 6. Heat capacities of a liquid, stable crystal, metastable crystal, and LQG of [bmp][Tf_2N]: circle, stable crystal; square, metastable crystal; triangle, liquid and LQG.

thermodynamic properties concerning the phase behavior are tabulated in Table 1 together with their literature values by adiabatic calorimetry.[36] Resultant standard thermodynamic quantities at round temperatures are tabulated in Table 3. There are no thermal anomalies in the liquid phase. The heat capacity of the liquid at 298.15 K ($C_{p,liq}$(298.15 K)) is 589.5 J K^{-1} mol^{-1} obtained from a linear regression of experimental heat capacities of the liquid.

The LQG of [bmp][Tf_2N] was formed by cooling at the cooling rate of ~1 K min^{-1} (quenched sample), and its glass transition temperature was 181 K as determined in the same manner as that for the LQG of [bmim][Tf_2N]. The annealed sample was prepared by annealing the quenched sample at 179 K. The heat capacity jump, slight heat capacity difference between quenched and annealed samples, and enthalpy relaxation due to the glass transition were also observed. $\Delta_{gl}C_p(T_g)$ and $\Delta_{gl}C_p(T_g)/C_p(LQG,T_g)$ of the quenched sample at T_g are 134 J K^{-1} mol^{-1} and 0.35, respectively.

An exothermic effect due to crystallization was observed above ~200 K upon heating the LQG. After annealing the sample until the exothermic effect due to the crystallization ceased, a metastable crystal phase was obtained. A broad thermal anomaly was observed for the metastable crystal at around 140 K, as shown in Figure 7. As the heat capacity around this thermal anomaly did not show thermal hysteresis, this thermal anomaly seems to arise from a second- or higher-

dx.doi.org/10.1021/jp210626v | J. Phys. Chem. B 2012, 116, 5406−5413

Table 3. Standard Thermodynamic Quantities of Stable Crystal and Liquid of [bmp][Tf$_2$N]

T/K	C_p/ J K^{-1} mol^{-1}	$[H(T) - H(0)]T^{-1}$/ J K^{-1} mol^{-1}	$[S(T) - S(0)]$/ J K^{-1} mol^{-1}	$-[G(T) - H(0)]T^{-1}$/ J K^{-1} mol^{-1}
		Crystal		
15	29.45	9.76	13.45	3.69
20	47.64	16.94	24.40	7.46
25	65.15	24.87	36.95	12.08
30	80.91	32.92	50.25	17.33
35	95.38	40.83	63.82	22.99
40	108.41	48.47	77.43	28.96
45	120.11	55.79	90.88	35.09
50	131.02	62.77	104.11	41.34
55	141.58	69.46	117.09	47.63
60	151.67	75.90	129.85	53.95
65	161.36	82.10	142.37	60.27
70	170.71	88.10	154.68	66.58
75	179.74	93.91	166.76	72.85
80	188.50	99.55	178.65	79.10
90	205.3	110.37	201.8	91.4
100	221.6	120.69	224.3	103.6
110	237.6	130.59	246.2	115.6
120	253.6	140.17	267.5	127.3
130	268.6	149.48	288.4	138.9
140	283.5	158.52	308.9	150.4
150	298.4	167.35	328.9	161.6
160	313.4	176.00	348.7	172.7
170	328.3	184.52	368.1	183.6
180	343.5	192.93	387.3	194.4
190	359.0	201.3	406.3	205.0
200	375.4	209.6	425.1	215.5
210	392.1	217.8	443.8	226.0
220	410.2	226.2	462.5	236.3
230	429.5	234.6	481.2	246.6
240	450.6	243.1	499.9	256.8
250	474.9	251.9	518.7	266.8
260	505.1	261.0	537.9	276.9
265.73	526.3	266.5	549.2	282.7
		Liquid		
265.73	568.6	349.1	631.8	282.7
270	571.4	352.6	640.8	288.2
280	578.0	360.5	661.7	301.2
290	584.3	368.1	682.1	314.0
300	590.6	375.4	702.0	326.6

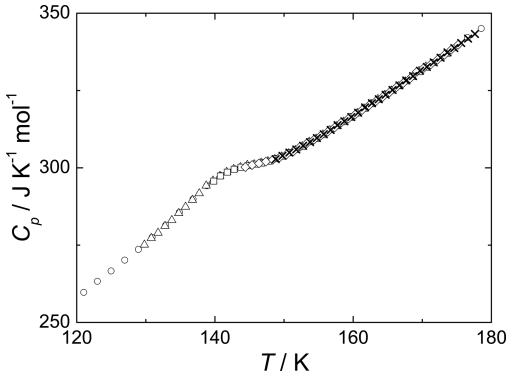

Figure 7. Heat capacities of a metastable crystal of [bmp][Tf$_2$N] with different thermal histories: circle, from 50 K; triangle, from 125 K; square, 139 K; diamond, from 144 K; cross, from 148 K.

order phase transition. The temperature, enthalpy, and entropy of the phase transition were 140 K, 200 J mol^{-1}, and 1.5 J K^{-1} mol^{-1}, respectively.

An exothermic effect due to a phase transition into the stable crystal phase was observed at around 210 K upon heating the metastable crystal. The heat capacity was measured from the lowest temperature for the stable crystal phase. Standard thermodynamic quantities given in Table 3 refer to this stable phase. Similarly to [bmim][Tf$_2$N], the thermal anomaly above 200 K varied depending on the thermal history (see Figures S3 and S4, Supporting Information). The stable crystal melted at 265.73 K. The enthalpy and entropy of fusion of the stable crystal of [bmp][Tf$_2$N] were 21.9 kJ mol^{-1} and 82.6 J K^{-1} mol^{-1}, respectively.

Although the glass transition related to the formation of LQG is not a main subject of this paper, some relevant quantities are given here. The methods to deduce these parameters are exactly the same as those in the previous paper on [hmim][Tf$_2$N].[27] The details are described in the Supporting Information. The size of the cooperatively rearranging region (CRR) in Adam–Gibbs theory of glass transition was deduced to be ∼4 from the configurational entropy (shown graphically in Figure S5, Supporting Information).[50−52] The residual entropy and Kauzmann temperature (T_K) were also determined to be 13 J K^{-1} mol^{-1} and 149 K, respectively. Fragility that characterizes non-Arrhenius behavior was deduced to be 8.4.[46] These parameters are comparable to those of [hmim][Tf$_2$N].[27] A symptom of the boson peak, which has been believed to be a common property of glass, was detected as a hump in the heat capacity difference between LQG and the stable crystal (Figure S6, Supporting Information).[53,54]

4. DISCUSSION

Comparison of Experimental and Predicted Properties. The heat capacity of [bmim][Tf$_2$N] at 298.15 K was predicted by GCM[8] to be 572.0 J K^{-1} mol^{-1}, and it deviated 1.1% from the present experimental results. Similarly, that is successfully predicted for [bmp][Tf$_2$N] by GCM[8] to be 585.9 J K^{-1} mol^{-1}, showing the deviation of 0.7%. On the other hand, predictions concerning the fusion are not so satisfactory. Lazzús reported the melting points of the two ionic liquids by GCM.[10] Calculated melting points of [bmim][Tf$_2$N] and [bmp][Tf$_2$N] are 282.01 and 315.89 K, respectively. Deviations between calculated and experimental melting points are more than 10 K. These deviations may be satisfactory for learning the trend of melting of the series of ionic liquids, but the accuracy is not sufficient for the comparison of melting points among individual ionic liquids like this study. Calculated properties by QSPR and molecular simulation also show similar trends to the case of GCM; these include good agreement in the heat capacities in contrast to large deviations in melting points.[20,21] The contrasting accuracies in predictions can be explained on the basis of the nature of predicted quantities. While the heat capacity is related only to one phase, properties of fusion concern the thermodynamic quantities of two phases. Even if the thermodynamic properties of a phase are well-predicted, a more accurate scheme for prediction is necessary for a phase transition. Note that this is true, irrespective of a prediction scheme such as GCM or QSPR.

Comparison of Heat Capacities. In the liquid phase (including the supercooled state), the heat capacity of [bmp][Tf$_2$N] is larger than that of [bmim][Tf$_2$N]. This can

dx.doi.org/10.1021/jp210626v | J. Phys. Chem. B 2012, 116, 5406−5413

be understood as the result of a larger number of atoms composing [bmp][Tf_2N] than [bmim][Tf_2N].

In the stable crystalline state, the heat capacity of [bmp][Tf_2N] is larger than that of [bmim][Tf_2N] in the vicinity of the fusion, as expected. However, the heat capacity of [bmp][Tf_2N] becomes smaller below 101 K, including lower temperatures below the glass transition toward the glassy crystal of [bmim][Tf_2N], as shown in Figure 8. The difference

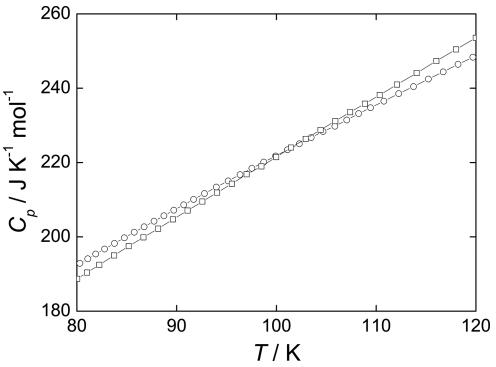

Figure 8. Heat capacities of crystalline [bmim][Tf_2N] and [bmp]-[Tf_2N] by adiabatic calorimetry around the intersection of heat capacities: circle, [bmim][Tf_2N]; square, [bmp][Tf_2N].

in the temperature dependence becomes significant in the vicinity of the fusion. The well-known case of increasing heat capacity near fusion is a premelting phenomenon. Taking the similar purities of the two ionic liquids (0.997 mol mol^{-1}) into consideration, however, this possibility is discarded. Another possible cause of the increase in the heat capacity is the contribution of thermal expansion because heat capacities by adiabatic calorimetry are essentially the heat capacities under constant pressure. The volumetric thermal expansion coefficient of the liquid is generally larger than that of the crystal. Consequently, the slope of the heat capacity due to thermal expansion of the liquid is steeper than that of the crystal. However, the slopes of the heat capacities of the liquid are not steeper than that of the crystal. Hence, the steeper increase in the heat capacity cannot be accounted for by the thermal expansion. Therefore, the present trend of the heat capacity of crystalline ionic liquids is to be regarded as the contributions of intermolecular and intramolecular vibrations.

Because the present ionic liquids share the common anion, the difference is expected for vibrational contributions of the cations. The frequencies of normal modes of [bmim]$^+$ and [bmp]$^+$ were evaluated by DFT calculations, accordingly. The calculated frequencies of the cations are tabulated in Table S1 (Supporting Information). The calculated frequencies for [bmim]$^+$ are quite similar to those for an ion pair, [bmim]·PF_6 by Talaty et al.,[55] except for the lowest-frequency region below ~100 cm^{-1}. Note that the low-frequency modes can affect the temperature dependence of the heat capacity at low temperatures but not that at high temperatures because of its saturation to the classical magnitude. Heat capacities of the two cations corresponding to the intramolecular vibration are estimated by using the calculated frequencies without a correction factor while assuming the harmonic oscillations (Einstein model), as shown in Figure 9. The calculated heat capacity of [bmp]$^+$ is smaller than those of *gauche*–*trans* and *trans*–*trans* [bmim]$^+$ at low temperature; then, the magnitude reverses at high temperatures. The crossing temperatures of

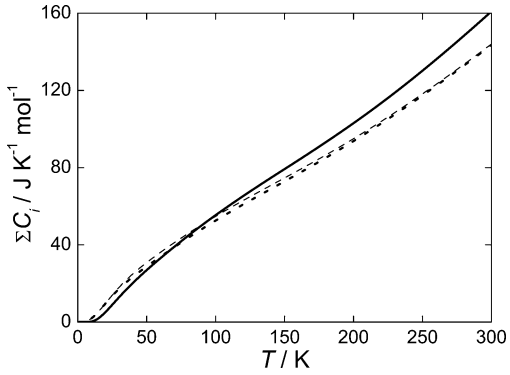

Figure 9. Heat capacities of [bmim]$^+$ and [bmp]$^+$ due to intramolecular vibrations by vibrational analyses: solid line, *gauche*–*trans* [bmim]$^+$; broken line, *trans*–*trans* [bmim]$^+$; dotted line, [bmp]$^+$.

gauche–*trans* and *trans*–*trans* [bmim]$^+$ are 68 and 93 K, respectively. The magnitudes and temperature dependences of the heat capacity of both conformations of [bmim]$^+$ seem reasonable in comparison with experimental results. Calculated heat capacities of [bmim]$^+$ will be discussed on the most stable conformation (*gauche*–*trans*) of [bmim]$^+$ because of the similar trends of calculated heat capacities between both conformations.

Comparison of Experimental and Calculated Heat Capacity Differences. Although the heat capacity difference between two ionic liquids is successfully explained at a qualitative level, we here proceed into more details. Figure 10

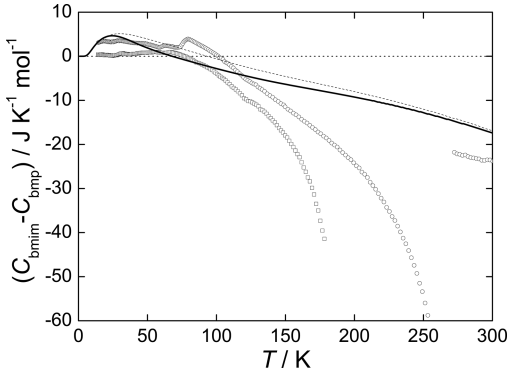

Figure 10. Heat capacity difference between [bmim][Tf_2N] and [bmp][Tf_2N] and that between [bmim]$^+$ and [bmp]$^+$: circle, heat capacity difference between [bmim][Tf_2N] and [bmp][Tf_2N] of the crystal and liquid phases; square, heat capacity difference between [bmim][Tf_2N] and [bmp][Tf_2N] of LQG; solid line, heat capacity difference between *gauche*–*trans* [bmim]$^+$ and [bmp]$^+$; broken line, heat capacity difference between *trans*–*trans* [bmim]$^+$ and [bmp]$^+$.

shows the temperature dependence of the differences between [bmim][Tf_2N] and [bmp][Tf_2N] obtained experimentally. Also shown is the difference between [bmim]$^+$ and [bmp]$^+$ through the DFT calculation. This comparison assumes a cancellation of contributions from the common anion [Tf_2N]$^-$. This assumption would not be perfect but seems acceptable.

In experimental heat capacity differences of the crystal phase, two humps at 59 and 73 K are due to glass transitions of the glassy crystal of [bmim][Tf_2N]. The heat capacity difference between crystalline [bmim][Tf_2N] and [bmp][Tf_2N] is positive below 101 K, turns into negative there, and becomes larger as the temperature increases. In LQG, heat capacity

dx.doi.org/10.1021/jp210626v | *J. Phys. Chem. B* 2012, 116, 5406–5413

differences below 75 K are almost zero and begin to decrease at 75 K. However, in the liquid phase, the deviation of [bmim][Tf_2N] from [bmp][Tf_2N] is distinctly enhanced compared to that in the crystal phase and LQG. In contrast, the calculated difference for $[bmim]^+$ and $[bmp]^+$ exhibits a smaller magnitude with a similar slope to the experimental one for liquids.

We discuss heat capacity differences in the liquid phase first. Needless to say, there is an intermolecular interaction among ions in the liquid phase. It is, therefore, no wonder that the temperature dependence of the heat capacity difference by adiabatic calorimetry deviates from that by vibrational analysis. However, those by adiabatic calorimetry and by vibrational analysis are certainly similar, as seen in Figure 10. This means that the dominant factor of heat capacity variation with temperature in the liquid phase is intramolecular vibration. The deviation in the absolute value of heat capacity differences (at the same temperature) is due to the difference in molecular motions beyond the intramolecular vibration. This is estimated from our previous study on [$C_n$mim][Tf_2N].[29] Heat capacities of the liquid at 298.15 K of [$C_n$mim][Tf_2N] have additivity concerning the alkyl chain length in the cation. The additivity was similar to the case of molecular liquids such as *n*-alkanes and 1-alkanols. The similarity of temperature dependence of the heat capacity except for the contribution of the intramolecular vibration of the cation means that [bmp][Tf_2N] has the same trend of thermodynamic behavior in the liquid phase as [$C_n$mim][Tf_2N] and other molecular liquids.

In contrast to the liquid, the trend of the experimental heat capacity difference in the crystal phase differs significantly from that of the calculated heat capacity difference. Although the crossing of heat capacities, though different in temperature, indicated that the temperature dependence of the heat capacity difference was dominated by intramolecular vibration at low temperatures, the trend of the difference in the experimental heat capacity deviates further from that of the calculated heat capacity as the temperature increases. Because the intermolecular interaction was not taken into account upon calculating the intramolecular vibrations, intermolecular interaction might cause some difference between experimental and calculated heat capacity differences. It is impossible to specify the contribution of intermolecular and intramolecular vibrations in the experimental heat capacity. The trend of the experimental heat capacity of the crystal phase, however, suggests two origins, enhancement of thermal excitation of intermolecular and/or intramolecular vibrations in [bmp][Tf_2N] and restriction of the thermal excitation of [bmim][Tf_2N]. It is easier to accept the restriction than the enhancement of molecular motion due to the intermolecular interaction. Besides, the restriction of molecular motion in crystalline [bmim][Tf_2N] is consistent with the low entropy of the crystal suggested in our previous study.[29]

Comparison of Thermodynamic Properties Associated with Fusion. In previous subsections, we discussed the intermolecular interaction based on molecular motion in the crystal and liquid independently through the comparison between the experimental and calculated heat capacity differences. In this subsection, differences between two ionic liquids are discussed by comparing thermodynamic quantities associated with fusion, which is a phase transition from the crystal phase to the liquid phase.

The melting point of [bmp][Tf_2N] is lower than that of [bmim][Tf_2N]. Both the enthalpy and entropy of fusion of [bmp][Tf_2N] are smaller than those of [bmim][Tf_2N], despite the disorder in the crystalline [bmim][Tf_2N] (as manifested by the occurrence of glass transitions). Because the melting point is given as a ratio between the enthalpy and entropy of fusion, a lower melting point of [bmp][Tf_2N] indicates that the smaller enthalpy of fusion dominates the melting point. The enthalpy of fusion consists of the "work" ($p\Delta V$) term associated with volume change and the change in internal energy required to release ions. More restricted molecular motion of [bmim][Tf_2N] in the crystal and similar molecular motion in the liquid require a larger fusion enthalpy in [bmim][Tf_2N] than that in [bmp][Tf_2N]. The relative magnitude of the enthalpy of fusion is consistent with the trend found in the comparison between experimental and calculated heat capacity differences.

In ionic liquids, Coulomb and van der Waals interactions work between ions. It is hard to assign the main difference in interaction between [bmp][Tf_2N] and [bmim][Tf_2N] to a van der Waals interaction because of the same alkyl groups in the cations. As for the Coulomb interaction, the delocalization of charge and the steric effect should be considered. Although the reduction in Coulomb interaction is caused by the delocalization of charge only in [bmim][Tf_2N], its enthalpy of fusion is larger than that of [bmp][Tf_2N]. Judging from the reduced enthalpy of fusion of [bmp][Tf_2N], the steric hindrance of methyl and butyl groups attached to the charged nitrogen atom in a pyrrolidinium ring is a dominant factor to weaken cation–anion interaction. The resultant weakened intermolecular interaction and "similar entropic" states (deduced through the comparison of the heat capacity of liquids in the previous subsection) leads to a lower melting point of [bmp][Tf_2N].

5. CONCLUSION

We have shown the heat capacities and thermodynamic properties of [bmim][Tf_2N] and [bmp][Tf_2N] by adiabatic calorimetry and contributions of the heat capacities of $[bmim]^+$ and $[bmp]^+$ due to intramolecular vibrations by vibrational analysis based on quantum chemical calculations. Through the comparison of thermodynamic properties between [bmim][Tf_2N] and [bmp][Tf_2N] and that between experimental and calculated heat capacity differences between $[bmim]^+$ and $[bmp]^+$, we have pointed out that the low melting points of the two ionic liquids are caused by intermolecular interaction in the crystal phase rather than in the liquid phase. The entropic effect dominates in [bmim][Tf_2N], whereas the enthalpic one does in crystalline [bmp][Tf_2N] for bringing their low melting points.

■ ASSOCIATED CONTENT

Supporting Information

Details of van't Hoff plots for cryoscopy, graphical presentation of history-dependent thermal anomalies of [bmp][Tf_2N], thermodynamic quantities of LQG, configurational entropy of [bmp][Tf_2N], heat capacity difference between LQG and the stable crystal of [bmp][Tf_2N], and results of vibrational analyses of $[bmim]^+$ and $[bmp]^+$. This material is available free of charge via the Internet at http://pubs.acs.org.

■ AUTHOR INFORMATION

Notes

The authors declare no competing financial interest.

■ ACKNOWLEDGMENTS

This work was partly supported by a Grant-in-Aid for Scientific Research on Priority Area 'Ionic Liquids' (No. 452/20031003) from the Ministry of Education, Culture, Sports, Science and Technology, Japan (MEXT).

■ REFERENCES

(1) Wilkes, J. S.; Zaworotko, M. J. *J. Chem. Soc., Chem. Commun.* **1992**, 965−967.
(2) Bonhôte, P.; Dias, A.-P.; Papageorgiou, N.; Kalyanasundaram, K.; Graetzel, M. *Inorg. Chem.* **1996**, *35*, 1168−1178.
(3) Ohno, H. *Bull. Chem. Soc. Jpn.* **2006**, *79*, 1665−1680.
(4) Katritzky, A. R.; Jain, R.; Lomaka, A.; Petrukhin, R.; Maran, U.; Karelson, M. *Cryst. Growth Des.* **2001**, *1*, 261−265.
(5) Krossing, I.; Slattery, J. M. *Z. Phys. Chem.* **2006**, *220*, 1343−1359.
(6) Rooney, D.; Jacquemin, J.; Gardas, R. *Top. Curr. Chem.* **2009**, *290*, 185−212.
(7) Aparicio, S.; Atilhan, M.; Karadas, F. *Ind. Eng. Chem. Res.* **2010**, *49*, 9580−9595.
(8) Gardas, R. L.; Coutinho, J. A. P. *Ind. Eng. Chem. Res.* **2008**, *47*, 5751−5757.
(9) Huo, Y.; Xia, S.; Zhang, Y.; Ma, P. *Ind. Eng. Chem. Res.* **2009**, *48*, 2212−2217.
(10) Lazzús, J. A. *Fluid Phase Equilib.* **2012**, *313*, 1−6.
(11) Katritzky, A. R.; Lomaka, A.; Petrukhin, R.; Jain, R.; Karelson, M.; Visser, A. E.; Rogers, R. D. *J. Chem. Inf. Comput. Sci.* **2002**, *42*, 71−74.
(12) Katritzky, A. R.; Jain, R.; Lomaka, A.; Petrukhin, R.; Karelson, M.; Visser, A. E.; Rogers, R. D. *J. Chem. Inf. Comput. Sci.* **2002**, *42*, 225−231.
(13) Eike, D. M.; Brennecke, J. F.; Maginn, E. J. *Green Chem.* **2003**, *5*, 323−328.
(14) Trohalaki, S.; Pachter, R.; Drake, G. W.; Hawkins, T. *Energy Fuels* **2005**, *19*, 279−284.
(15) Sun, N.; He, X.; Dong, K.; Zhang, X.; Lu, X.; He, H.; Zhang, S. *Fluid Phase Equilib.* **2006**, *246*, 137−142.
(16) López-Martin, I.; Burello, E.; Davey, P. N.; Seddon, K. R.; Rothenberg, G. *ChemPhysChem* **2007**, *8*, 690−695.
(17) Varnek, A.; Kireeva, N.; Tetko, I. V.; Baskin, I. I.; Solov'ev, V. P. *J.Chem. Inf. Model.* **2007**, *47*, 1111−1122.
(18) Bini, R.; Chiappe, C.; Duce, C.; Micheli, A.; Solaro, R.; Starita, A.; Tiné, M. R. *Green Chem.* **2008**, *10*, 306−309.
(19) McLeese, S. E.; Eslick, J. C.; Hoffmann, N. J.; Scurto, A. M.; Camarda, K. V. *Comput. Chem. Eng.* **2010**, *34*, 1476−1480.
(20) Cadena, C.; Zhao, Q.; Snurr, R. Q.; Maginn, E. J. *J. Phys. Chem. B* **2006**, *110*, 2821−2832.
(21) Jayaraman, S.; Maginn, E. J. *J. Chem. Phys.* **2007**, *127*, 214504.
(22) Maginn, E. J. *J. Phys.: Condens. Matter* **2009**, *21*, 373101.
(23) Nieto, d. C. C. A. *J. Mol. Liq.* **2010**, *156*, 10−17.
(24) Marsh, K. N.; Brennecke, J. F.; Chirico, R. D.; Frenkel, M.; Heintz, A.; Magee, J. W.; Peters, C. J.; Rebelo, L. P. N; Seddon, K. R.; Rossi, M. J.; et al. *Pure Appl. Chem.* **2009**, *81*, 781−790.
(25) Chirico, R. D.; Diky, V.; Magee, J. W.; Frenkel, M.; Marsh, K. N.; Rossi, M. J.; McQuillan, A. J.; Lynden-Bell, R. M.; Brett, C. M. A.; Dymond, J. H.; et al. *Pure Appl. Chem.* **2009**, *81*, 791−828.
(26) Matsumoto, K.; Hagiwara, R. *J. Fluorine Chem.* **2007**, *128*, 317−331.
(27) Shimizu, Y.; Ohte, Y.; Yamamura, Y.; Saito, K.; Atake, T. *J. Phys. Chem. B* **2006**, *110*, 13970−13975.
(28) Shimizu, Y.; Ohte, Y.; Yamamura, Y.; Saito, K. *Chem. Lett.* **2007**, *36*, 1484−1485.
(29) Shimizu, Y.; Ohte, Y.; Yamamura, Y.; Saito, K. *Chem. Phys. Lett.* **2009**, *470*, 295−299.
(30) MacFarlane, D. R.; Meakin, P.; Sun, J.; Amini, N.; Forsyth, M. *J. Phys. Chem. B* **1999**, *103*, 4164−4170.
(31) Matsumoto, H.; Sakaebe, H.; Tatsumi, K. *J. Power Sources* **2005**, *146*, 45−50.
(32) Tokuda, H.; Ishii, K.; Susan, M. A. B. H.; Tsuzuki, S.; Hayamizu, K.; Watanabe, M. *J. Phys. Chem. B* **2006**, *110*, 2833−2839.
(33) Gomes de Azevedo, R.; Esperança, J. M. S. S.; Szydlowski, J.; Visak, Z. P.; Pires, P. F.; Guedes, H. J. R.; Rebelo, L. P. N *J. Chem. Thermodyn.* **2005**, *37*, 888−899.
(34) Pereiro, A. B.; Veiga, H. I. M.; Esperança, J. M. S. S.; Rodríguez, A. *J. Chem. Thermodyn.* **2009**, *41*, 1419−1423.
(35) Blokhin, A. V.; Paulechka, Y. U.; Strechan, A. A.; Kabo, G. J. *J. Phys. Chem. B* **2008**, *112*, 4357−4364.
(36) Paulechka, Y. U.; Kabo, A. G.; Blokhin, A. V.; Kabo, G. J.; Shevelyova, M. P. *J. Chem. Eng. Data* **2010**, *55*, 2719−2724.
(37) Tsuzuki, S.; Tokuda, H.; Hayamizu, K.; Watanabe, M. *J. Phys. Chem. B* **2005**, *109*, 16474−16481.
(38) Valkenburg, M. E. V.; Vaughn, R. L.; Williams, M.; Wilkes, J. S. *Thermochim. Acta* **2005**, *425*, 181−188.
(39) Forsyth, S.; Golding, J.; MacFarlane, D. R.; Forsyth, M. *Electrochim. Acta* **2001**, *46*, 1753−1757.
(40) Preston-Thomas, H. *Metrologia* **1990**, *27*, 3−10.
(41) Frisch, M. J.; Trucks, G. W.; Schlegel, H. B.; Scuseria, G. E.; Robb, M. A.; Cheeseman, J. R.; Montgomery, Jr., J. A.; Vreven, T.; Kudin, K. N.; Burant, J. C. et al. *Gaussian 03*, revision E.01; Gaussian, Inc.: Wallingford, CT, 2004.
(42) Tsuzuki, S.; Arai, A. A.; Nishikawa, K. *J. Phys. Chem. B* **2008**, *112*, 7739−7747.
(43) Although the measurement of heat capacities in the adiabatic calorimeter is done under neither constant pressure nor constant volume condition, the resultant heat capacities can be treated as that under constant pressure C_p because of small compressibility of condensed phases (liquid and solid). The phase transition from the crystal to liquid occurs under a condition different from that under ambient pressure. The transition is hence termed "fusion" in this paper. On the other hand, the temperatures of transition determined in the present experiments are very close (identical within experimental accuracy) to those under the normal condition as readily estimated using the Clapeyron relation. The experimental temperature of transition is thus identified as a "melting point" under the ambient condition.
(44) Tunnicliff, D. D.; Stone, H. *Anal. Chem.* **1955**, *27*, 73−80.
(45) Mastrangelo, S. V. R.; Dornte, R. W. *J. Am. Chem. Soc.* **1955**, *77*, 6200−6201.
(46) Angell, C. A. *J. Non-Cryst. Solids* **1991**, *131*−*133*, 13−31.
(47) Adachi, K.; Suga, H.; Seki, S. *Bull. Chem. Soc. Jpn.* **1968**, *41*, 1073−1087.
(48) Paulechka, Y. U.; Kabo, G. J.; Blokhin, A. V.; Shaplov, A. S.; Lozinskaya, E. I.; Golovanov, D. G.; Lyssenko, K. A.; Korlyukov, A. A.; Vygodskii, Y. S. *J. Phys. Chem. B* **2009**, *113*, 9538−9546.
(49) Sakka, S.; Mackenzie, J. D. *J. Non-Cryst. Solids* **1971**, *6*, 145−162.
(50) Adam, G.; Gibbs, J. H. *J. Chem. Phys.* **1965**, *43*, 139−146.
(51) Yamamuro, O.; Tsukushi, I.; Lindqvist, A.; Takahara, S.; Ishikawa, M.; Matsuo, T. *J. Phys. Chem. B* **1998**, *102*, 1605−1609.
(52) Atake, T.; Abe, R.; Honda, K.; Kawaji, H.; Johnsen, H. B.; Stølen, S. *J. Phys. Chem. Solids* **2000**, *61*, 1373−1377.
(53) Yamamuro, O.; Takeda, K.; Tsukushi, I.; Matsuo, T. *Physica B* **2002**, *311*, 84−89.
(54) Saito, K.; Kobayashi, H.; Miyazaki, Y.; Sorai, M. *Solid State Commun.* **2001**, *118*, 611−614.
(55) Talaty, E. R.; Raja, S.; Storhaug, V. J.; Dölle, A.; Carper, W. R. *J. Phys. Chem. B* **2004**, *108*, 13177−13184.